AIP | Review of Scientific Instruments

Invited Article: First flight in space of a wide-field-of-view soft x-ray imager using lobster-eye optics: Instrument description and initial flight results

Michael R. Collier, F. Scott Porter, David G. Sibeck, Jenny A. Carter, Meng P. Chiao, Dennis J. Chornay, Thomas E. Cravens, Massimiliano Galeazzi, John W. Keller, Dimitra Koutroumpa, Joseph Kujawski, Kip Kuntz, Andy M. Read, Ina P. Robertson, Steve Sembay, Steven L. Snowden, Nicholas Thomas, Youaraj Uprety, and Brian M. Walsh

Citation: Review of Scientific Instruments **86**, 071301 (2015); doi: 10.1063/1.4927259
View online: http://dx.doi.org/10.1063/1.4927259
View Table of Contents: http://scitation.aip.org/content/aip/journal/rsi/86/7?ver=pdfcov
Published by the AIP Publishing

Invited Article: First flight in space of a wide-field-of-view soft x-ray imager using lobster-eye optics: Instrument description and initial flight results

Michael R. Collier,[1,a)] F. Scott Porter,[1,b)] David G. Sibeck,[1,c)] Jenny A. Carter,[2,d)] Meng P. Chiao,[1,e)] Dennis J. Chornay,[1,f)] Thomas E. Cravens,[3,g)] Massimiliano Galeazzi,[4,h)] John W. Keller,[1,i)] Dimitra Koutroumpa,[5,j)] Joseph Kujawski,[6,k)] Kip Kuntz,[7,l)] Andy M. Read,[2,m)] Ina P. Robertson,[3,n)] Steve Sembay,[2,o)] Steven L. Snowden,[1,p)] Nicholas Thomas,[1,q)] Youaraj Uprety,[4,r)] and Brian M. Walsh[8,s)]

[1]*NASA/Goddard Spaceflight Center, Greenbelt, Maryland 20771, USA*
[2]*The Department of Physics and Astronomy, The University of Leicester, Leicester LE1 7RH, United Kingdom*
[3]*Department of Physics and Astronomy, University of Kansas, 1251 Wescoe Hall Dr., Lawrence, Kansas 66045, USA*
[4]*Department of Physics, University of Miami, Coral Gables, Florida 33124, USA*
[5]*CNRS/INSU, LATMOS-IPSL, Université Versailles St-Quentin, Sorbonne Universités, UPMC Univ. Paris 06, 11 Boulevard d'Alembert, 78280 Guyancourt, France*
[6]*Department of Physics, Siena College, Loudonville, New York 12211, USA*
[7]*The Henry A. Rowland Department of Physics and Astronomy, The Johns Hopkins University, Baltimore, Maryland 21218, USA*
[8]*Space Sciences Laboratory, University of California, Berkeley, California 94720, USA*

(Received 20 March 2015; accepted 1 July 2015; published online 28 July 2015)

We describe the development, launch into space, and initial results from a prototype wide field-of-view soft X-ray imager that employs lobster-eye optics and targets heliophysics, planetary, and astrophysics science. The sheath transport observer for the redistribution of mass is the first instrument using this type of optics launched into space and provides proof-of-concept for future flight instruments capable of imaging structures such as the terrestrial cusp, the entire dayside magnetosheath from outside the magnetosphere, comets, the Moon, and the solar wind interaction with planetary bodies like Venus and Mars [Kuntz *et al.*, Astrophys. J. (in press)]. © *2015 AIP Publishing LLC.* [http://dx.doi.org/10.1063/1.4927259]

I. INTRODUCTION

The solar wind plasma flows continuously from all latitudes and longitudes on the sun occupying the entire heliosphere and interacting with the neutral gas inside it. Although the solar wind is mostly protons, it also contains a flux ($>10^5/cm^2/s$) of high charge state heavy ions such as O^{+7}. When these high charge state heavy ions interact with neutral gas, many undergo charge exchange reactions, acquiring an electron. Almost immediately afterwards, the high charge state ions emit soft (below a couple of keV) X-ray photons.[1,2]

This process is known as soft X-ray emission due to solar wind charge exchange, or SWCX, recombination and it occurs throughout the solar system and beyond: in planetary atmospheres, comets, interplanetary space, Earth's exosphere, and likely in supernova remnants and other regions where astrophysical plasmas interact with the neutral interstellar medium. The study of SWCX is truly cross-disciplinary.

Relevance to Heliophysics: The terrestrial magnetic field carves a cavity in the solar wind known as the magnetosphere. All of the mass, momentum, and energy powering geomagnetic storms are supplied by the solar wind. Because geomagnetic storms are responsible for some of the most severe space weather disturbances, accurate forecasts from global numerical simulations that incorporate the fundamental physics are essential.

This kind of a predictive capability requires a global view generated on a short cadence of the overall interaction at the magnetopause, the outer boundary of the magnetosphere. Although we have had many years of *in-situ* spacecraft observations,[3] from which we have learned a great deal, these measurements are sporadic and single-point. The necessary input for large-scale models requires simultaneous global observations of the magnetopause and magnetosheath.[4] Significant SWCX emission originates from the magnetosheath and deep within the magnetospheric cusps because in these locations the solar wind encounters Earth's neutral exosphere. Furthermore, these regions map out and provide boundary conditions for the Earth's magnetosphere.

[a)]michael.r.collier@nasa.gov
[b)]frederick.s.porter@nasa.gov
[c)]david.g.sibeck@nasa.gov
[d)]jac48@leicester.ac.uk
[e)]meng.p.chiao@nasa.gov
[f)]dennis.j.chornay@nasa.gov
[g)]cravens@ku.edu
[h)]galeazzi@physics.miami.edu
[i)]john.w.keller@nasa.gov
[j)]dimitra.koutroumpa@latmos.ipsl.fr
[k)]jkujawski@siena.edu
[l)]kuntz@pha.jhu.edu
[m)]amr30@leicester.ac.uk
[n)]robertin@ku.edu
[o)]sfs5@leicester.ac.uk
[p)]steven.l.snowden@nasa.gov
[q)]nicholas.e.thomas@nasa.gov
[r)]ubaraj@physics.miami.edu
[s)]bwalsh@ssl.berkeley.edu

Both observations[5,6] and simulations[7] indicate that SWCX soft X-ray imaging will produce global images of the solar wind-magnetosphere interaction.

Relevance to Planetary Science: As comets approach the sun, they sublimate large clouds of neutral gas. The solar wind interacts with these clouds in a complex process that has been imaged and studied using soft X-ray emission.[2,8–10]

The solar wind-planetary body interaction can also be imaged for non-magnetized planets. Both Mars and Venus show global SWCX soft X-ray emissions from their exospheres that are similar in nature to the emission from Earth, demonstrating both the feasibility of global magnetosheath imaging at Earth and that SWCX soft X-ray imaging will be a valuable part of future planetary missions. Chandra observations in 2001 revealed a SWCX X-ray halo around Mars,[11–15] while Chandra observations in 2006/2007 detected SWCX soft X-rays from the Cytherian (i.e., Venusian) exosphere.[16,17]

Soft X-rays have also been detected from the interaction between the solar wind and the tenuous lunar exosphere.[18]

Relevance to Astrophysics: All soft X-ray observations from X-ray observatories must contend with a significant spatially, temporally, and spectrally changing foreground from SWCX emission originating in the solar system.[19,20] The correct interpretation of observations, particularly those of extended objects and the diffuse X-ray background, requires understanding and accurate modeling of this foreground emission. For example, significant amounts of observing time on Chandra, XMM-Newton, Suzaku, and ROSAT have been adversely affected by this emission, and scientific interpretation errors have occurred because of our lack of understanding of SWCX.[21] Only when we understand this phenomenon fully will we be able to maximize the return on investment for these NASA, ESA, and JAXA missions.

In this paper, we report on the design, development, and launch into space of a wide field-of-view (FOV) laboratory prototype instrument designed to image soft X-ray emission associated with the solar wind's interaction with terrestrial and planetary neutral atoms. Although observations with astrophysics telescopes of SWCX emission near Earth and around Mars and Venus demonstrate the feasibility of global imaging, a wide FOV imager is needed to study the important large-scale solar wind interactions (current astrophysics telescopes have FOVs $\lesssim 0.5°$).

II. PROTOTYPE INSTRUMENT

A. Lobster-eye optics

There exists a wide variety of instrumental approaches to imaging soft X-rays. The conventional nested mirror optics used by many X-ray telescopes are designed to image point or relatively compact sources within a small field-of-view. This approach will not work for objects such as the magnetosheath and cusps, the scientific targets of some planned missions, because of their proximity and scale. Instead, a different approach using an alternative wide optic technology like the micropore (lobster-eye) optical element developed by the University of Leicester[22,23] must be employed in an X-ray camera designed to image these targets globally.

STORM (Sheath Transport Observer for the Redistribution of Mass) was flown as a piggyback experiment on the Diffuse X-ray emission from the Local galaxy (DXL) sounding rocket mission.[24] DXL/STORM uses slumped microchannel plates (MCPs) with square channels, called micropore reflectors (MPRs), that deliver wide field-of-view with low mass. Each spatial dimension of the square pores on these MPRs is nominally 20 μm. These pores form an array of channels approximating, in a small area to increase the reflecting surface and thus the effective area of the optic, a Kirkpatrick/Baez system.[25]

Slumping the MPR so that the channel axes are perpendicular to the surface of a sphere causes reflected X-rays from infinity to focus on an image surface at half the sphere's radius.[26] (See Figure 1 of Collier *et al.*[27] for a diagram illustrating the principle of operation of a wide angle soft X-ray camera.) Focusing occurs when an X-ray photon reflects from two orthogonal walls of the channel.

MPRs will fly as the focusing element of the University of Leicester's Mercury Imaging X-ray Spectrometer (MIXS) on the BepiColombo mission to Mercury.[28,29]

B. Optics assembly

The DXL/STORM camera employs an optics holder that accommodates up to nine 4 cm × 4 cm slumped micropore reflectors manufactured by Photonis Corporation (see Figure 1). The entire assembly with all facets populated has about a 9.2° field-of-view, side-to-side. However, because of cost constraints, only the central facet and one adjacent facet were populated. The remaining facets contained aluminum blanks. Furthermore, the response of the populated non-central facet was partially cut off by the edge of the detector plane position sensing anode board.

The reflectors have a 75 cm radius of curvature and a 37.5 cm focal length. The micropore reflectors were flown uncoated. In future instruments, coating will increase the MPR reflectivity.

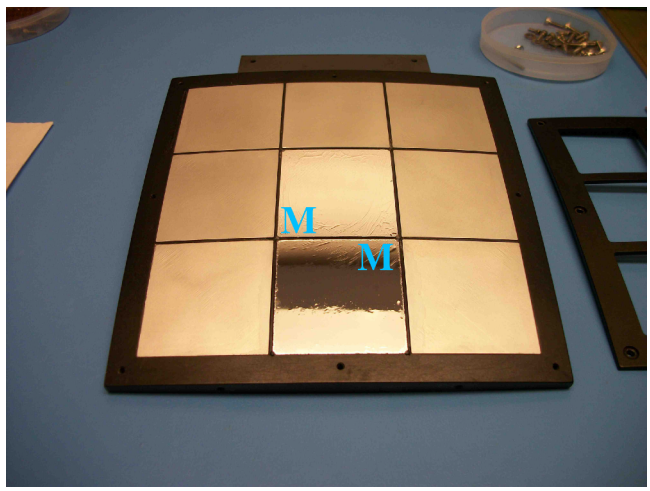

FIG. 1. The 3×3 optics holder accommodates up to nine 4 cm×4 cm micropore reflectors with about a 9.2° FOV, side-to-side. DXL/STORM was flown with two micropore reflector slots populated, as shown in the figure (labeled "M"), with the others covered by aluminum blanks.

The MPRs generate a cross-shaped point spread function (PSF) with the legs resulting from photon reflections off one pore wall and the central focus resulting from photon reflections off two adjacent pore walls. (See Figure 7 of Branduardi-Raymont *et al.*[30]) Qualitatively, the effective area versus energy plot resembles that of Figure 9 of Branduardi-Raymont *et al.*[30] with a peak near 1 keV, falling off significantly by about 0.1 keV at the lower energies and by about 2 keV at the higher energies.

The angular resolution of DXL/STORM was limited by the spatial resolution of the position-sensing to about 0.3° although the angular resolution of the MPRs is significantly better by about an order of magnitude.[30]

The micropore optics holder, shown in Figure 1, is machined to the shape of a portion of a 75 cm radius sphere. The holder was populated with two of the 75 cm radius of curvature micropore reflectors bonded with filters: one in the center and one on the edge with the remaining seven pockets populated with aluminum blanks machined to the same shape as the micropore reflectors. The micropore reflectors and blanks were attached to the optics holder using a mixture of uralane 5750 and 6% cabosil by weight. A thin mask sits over the micropore reflector and blanks. The aluminum optics holder and mask are black anodized for stray light suppression.

Luxel Corporation filters constructed of a 2179 Å polyimide layer for UV suppression and a 307 Å aluminum layer for visible suppression were mounted on top of the two micropore reflectors. The MPRs served as a convenient "mesh" for supporting the filter. This approach proved superior to the standard practice of mounting the filters on a nickel mesh above the detector plane by eliminating the transmission lost to the mesh.

To test the bond between the UV filter and the micropore reflector, we performed ten thermal cycles on the filter-bonded MPR in a vacuum oven. The MPR spent 325 h 48 min above a temperature of 37.8 °C and the maximum measured temperature on the MPR (using a thermocouple) was 185.8 °C. The MPR was held at this maximum temperature for 21 h 6 min. Over the entire testing, no visible change in the UV filter or MPR was observed nor in subsequent testing was there any evidence of a physical change.

In addition, in July 2012, we shake-tested the integrated DXL/STORM instrument at Wallops Flight Facility with the UV filter attached to the micropore reflector in part to test how robust the filter mounting was. In this test, we used the Black Brant IX vibration specifications including a sine sweep in the thrust axis and random in all three axes at 12.7 g rms. The micropore reflector, attached UV filter, MCP detector plane plates, and all electronics survived flight level vibration.

C. Sensitivity to energetic particles

Protons and electrons moving in the direction of the camera optics that manage to penetrate the UV filter, avoid being scattered into the micropore walls, and end up on a trajectory towards the detector plane MCP can produce counts that are indistinguishable from X-rays. Unless the beam consists of extremely high energy unidirectional particles, these counts will appear as a uniform background on the detector plane.

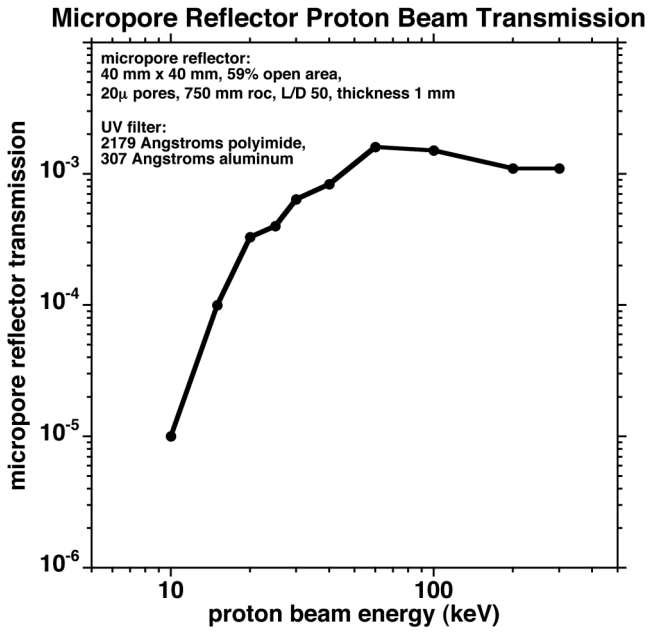

FIG. 2. The instrument response efficiency for protons impinging directly on the micropore reflector as a function of beam energy.

We tested the micropore reflector and UV filter energetic proton suppression at the GSFC radiation facility, and the results are shown in Figure 2. The geometry of the MPR itself suppresses the flux by a factor of 10^3 as evidenced by the flattening of the curve with energy at high energies. At the lowest energy tested, 10 keV, the filter provides an additional factor of 10^2 suppression.

X-ray astronomers are very familiar with electron contamination and have been protecting against it for nearly five decades. Magnetic brooms are the standard mechanism.[31] Furthermore, DXL/STORM's filters are able to stop electrons with energies less than about 3.4 keV. DXL/STORM launched from White Sands Missile Range where electron contamination is insignificant even without sweeper magnets. If the launch were to occur at a site where electron contamination is significant, calculations show that magnetic fields of only a couple hundred gauss (which are easily achieved) would be sufficient to eliminate electron contamination.

D. Detector and electronics

The DXL/STORM detector plane is shown in Figure 3. It mounts directly to the top of the electronics box. The assembly employs a chevron configuration microchannel plate stack coated with KBr for enhanced soft X-ray sensitivity over a wedge-and-strip geometry anode board for position sensing.

The wedge and strip anode approach[32] employs an anode board with interlaced pairs of wedges and strips. The wedge points are oppositely directed in each pair and the strip widths gradually change from small to large for one set and from large to small for the other set. The location that an X-ray photon hits the detector plane is determined by using the ratio of the amplitudes of the two signals from the wedges, defining the position along one axis, and the ratio of the amplitudes of the two signals from the strips, defining the position along the

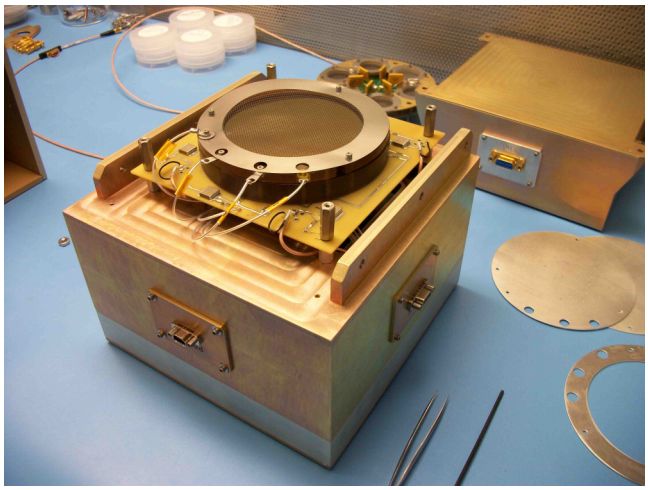

FIG. 3. The detector plane is a wedge and strip anode behind a chevron stack of MCPs coated with KBr for improved soft X-ray response. The anode board is mounted on top of the electronics box.

other axis. The resolution of the DXL/STORM anode board is about two millimeters. Although this resolution has been improved on subsequent prototypes since the DXL/STORM launch, it was more than sufficient for the DXL/STORM application, providing about 0.3° angular resolution.

The electronics for the DXL/STORM soft X-ray camera include an anode board, preamplifier and peak-hold board, Low Voltage Power Supply (LVPS) board, High Voltage Power Supply (HVPS) board, and Command and Data Handling (C&DH) board.

The DXL/STORM instrument is powered by an unregulated 28 V nominal line supplied on a nine pin Micro-D Metal shell (MDM) connector which goes directly to a DC-DC converter board. This board which employs two Virginia Power Technology converters and a filter produces the required voltages, 12 V, 5 V, 3.3 V, and 2.2 V, to power the HVPS and peak-hold boards as well as the C&DH board and its Field-Programmable Gate Array (FPGA).

The high voltage is supplied to the microchannel plate stack by a HVPS board employing an EMCO Corporation C50 supply controlled by a 0-5 V analog voltage with a voltage divider resistor chain to generate the specific voltages required for each stage in the MCP stack.

The four raw signals that determine the photon position are processed by a peak-hold/preamp board generating a square pulse output proportional to the amplitude of the raw signals. These pulses are then fed into analog-to-digital converters (ADCs) on the C&DH board and read by its FPGA.

The C&DH board reads the data from the anode board, formats it, attaches a time tag, and stores the data on electrically erasable/programable read-only memories (EEPROMs) located on the board itself. In addition, the C&DH board was designed, upon sensing an external pin transitioning from 0 to 5 V, to begin autonomously ramping up the high voltage on the MCP stack according to a user-defined time table and start acquiring data. This approach was implemented to minimize requirements on rocket systems. After the instrument was recovered following launch, the flight data were downloaded from the EEPROMs.

All the electronics boards are integrated into a single electronics box shown in Figure 3. This box has three connectors: one 9-pin MDM connector for power, one 15-pin MDM connector for the signals, and a third 9-pin MDM connector functioning as a high voltage disable plug that shorts out the 12 V supplying power to the HVPS board to eliminate the possibility of arcing if the high voltage is accidentally turned on while testing in air.

E. Integration and testing

The assembled instrument is shown in Figure 4. Both the instrument housing and the instrument electronics box are fabricated from aluminum and plated with gold iridite. The small black anodized assemblies visible on the top and sides of the instrument are vents to ensure trapped gas in the instrument does not compromise the rapid turn-on of the MCP high voltages during the flight or apply pressure to the UV filters. Further assisting this effort, DXL/STORM was launched under vacuum in its own vacuum section on the rocket. The vacuum section door was opened to space before the high voltage was turned on. Additional vents are present on the electronics box at the rear of Figure 4. The instrument also accommodates a purge fitting to allow dry nitrogen to flow through the inside to ensure the instrument remains clean and the MCPs remain dry. Table I lists the flight unit specifications.

For testing purposes, a six foot beam tube was mounted to a 2.75 in. conflat flange on a vacuum chamber large enough to accommodate the entire instrument. This setup achieved vacuum levels in the 10^{-7} Torr range. A gate valve with a Be window on the end of the beam tube allowed instrument testing with an 85 μCi Fe^{55} source as well as an Oxford soft X-ray source providing 1.49 keV (Al) X-rays.

The micropore reflector generates a cross pattern on the detector plane in response to a point source at infinity. Although our testing setup was not long enough to generate X-rays sufficiently parallel to provide a true parallel-beam

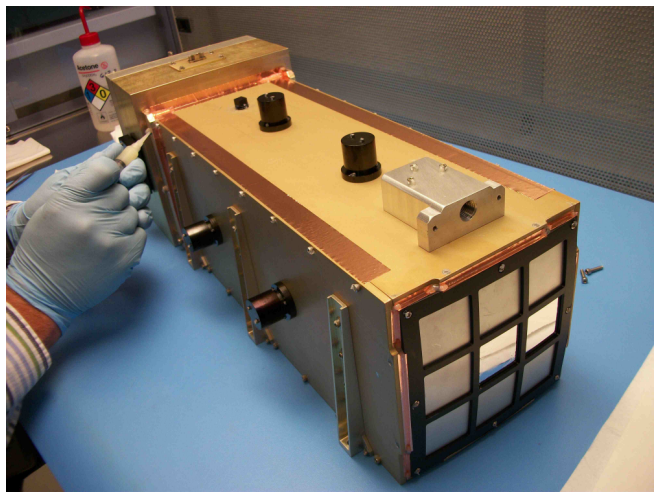

FIG. 4. The integrated instrument prototype with the optics assembly at the front and the electronics box in the back. The electronics box includes the anode, peak-hold, LVPS, HVPS, and C&DH boards.

TABLE I. DXL/STORM flight unit specifications.

Resource	Value
Mass	7.7 kg
Power	4.2 W
Field-of-view	9.2°×9.2° (~6°×3° populated)
Envelope	189×219×520 mm
Data rate	~7.2 kBps (stored internally)

characterization of the optics, we still observed a cross-like pattern on the position-sensing anode.

III. DXL LAUNCH OVERVIEW

The DXL/STORM instrument[27] launched as a piggyback experiment on the DXL mission[33,34] on 12 December 2012 at 10:20 P.M. local time on a Black Brant IX rocket from White Sands Missile Range. DXL/STORM began collecting data in its nominal science mode (i.e., at the maximum MCP gain corresponding to about 2300 V between the ground grid and the anode) for 254 s starting at launch plus 154 s (~190 km altitude upward moving). Data collection continued through apogee at about launch plus 260 s (~250 km altitude) to launch plus 408 s (~140 km altitude downward moving).

Although the Black Brant rocket used for this launch experienced "serious thrust anomalies" that saturated the accelerometers at 25 g (random vibration testing was done at 12.7 g) and caused the Sounding Rocket Program Office to suspend all Brant flights for a period, both DXL and DXL/STORM survived the rough ride and functioned nominally. In particular, the micropore reflectors and the UV filters mounted on them were perfectly intact when the instrument was recovered.

The main DXL payload consisting of two proportional counters looked anti-sunward to detect soft X-ray SWCX emission from the helium focusing cone.[19] The DXL/STORM instrument looked out the back of the rocket on a mounting plate canted by 7.4°. The cant was introduced so that, as the payload rotated, the STORM field-of-view would scan regions with different surface brightnesses. This variability would allow separation between cosmic photons and instrumental backgrounds. Thus, STORM's FOV was an annulus, centered on l = −229.9°, b = 65.9° (RA = 11.24 h, Dec = 18.06°), and 7.4° wide. In a magnetospheric geometry, the rocket was on the nightside behind the terminator with DXL/STORM looking dawnward towards the flank magnetosheath.

This observing direction is not optimal for detecting magnetosheath solar wind charge exchange which peaks at the dayside nose of the magnetopause.[35] Nevertheless there is non-negligible emission on the flanks of the magnetosheath even during typical solar wind conditions.[18,36] Consequently, DXL/STORM was observing some SWCX emission from the magnetosheath.

Over the course of the flight, the DXL rocket executed four sky scans rotating the DXL FOV through the direction of the helium focusing cone and back again twice. Between sky scans two and three, the DXL rocket executed an Earth scan during which the DXL FOV passed through nadir. Because DXL/STORM looked out the back of the rocket, during this period its FOV scanned close to the horizon.

IV. CALCULATION OF EXPECTED DXL/STORM RATE FROM THE COSMIC BACKGROUND

In this section, we estimate the expected DXL/STORM count rate based on the ROSAT PSPC All-Sky Survey-characterized background in the direction DXL/STORM was observing. We have assumed a typical soft X-ray background spectrum[37] normalized by the measured soft X-ray background flux in the 0.111-0.284 keV (R12) band from ROSAT. We expect the cosmic flux in DXL/STORM's field-of-view to vary with the rocket roll angle from ~113 photon/cm^2/s/sr to 180 photon/cm^2/s/sr with an average of about 124 photon/cm^2/s/sr through the annulus covered by the field-of-view.

The conversion from the normalized background spectrum to DXL/STORM count rate assumed a single 4 cm × 4 cm facet covering a 3° × 3° field-of-view for a solid angle of 2.7×10^{-3} sr. The physical collecting area of the facet is 16 cm^2, and the transparency of the micropore reflector is, based on Photonis specifications, (at least) 60%, so that the actual collecting area is 9.6 cm^2. The Luxel UV filter bonded to the front face of the micropore reflector has a 2179 Å polyimide layer and a 307 Å aluminum layer. At 250 eV, this filter has a transmission of about 70%, so that with the filter, the effective area is 6.7 cm^2. Based on Pearce *et al.*,[38] Figure 7, the detector plane microchannel plate efficiency is about 0.4. Thus, the total effective area of the micropore reflector is about 2.7 cm^2. Consequently, the count rate, R, expected is about R = 124 photon/cm^2/s/sr · 2.7×10^{-3} sr · 2.7 cm^2 = 0.90 s^{-1}. This count rate will appear in the 20 mm × 20 mm region on the detector plane that results from the focusing of the photons that hit the 4 cm × 4 cm micropore reflector.

This represents the minimum predicted soft X-ray flux DXL/STORM observes because (i) it does not include the SWCX component, only cosmic background, (ii) only one facet was assumed populated while two were flown, and (iii) the micropore reflector transparency is a lower limit.

V. LIGHT CURVE OBSERVATIONS

Figure 5 shows, in the top panel, the counts collected during the flight while DXL/STORM was operating at its maximum MCP gain level. The central facet position is indicated by the large white central box while the four boxes at the corners were used to evaluate the background level. For comparison, the lower panel shows the results of a vacuum sequence test on the ground during which the DXL/STORM rocket section door was closed and no soft X-rays are expected to be observed.

Figure 6 shows the observed DXL/STORM light curve during the DXL rocket flight. The red curve shows the light curve from the central populated facet, counts per second observed in the 20 mm × 20 mm region of the detector plane corresponding to the central facet averaged over 5 s. The blue

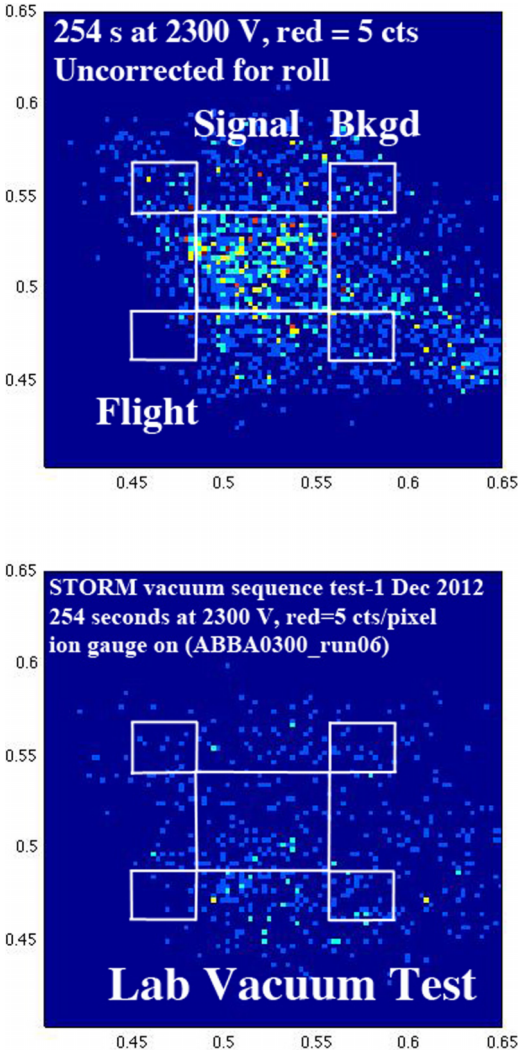

FIG. 5. Top panel: The raw DXL/STORM counts in detector coordinates. Bottom panel: The DXL/STORM response during a vacuum sequence test when the instrument's rocket section door was closed and no soft X-rays were present.

curve on Figure 6 shows the estimated noise count rate upper limit due to dark current and particle counts. We estimate that this rate is about 0.6 Hz, indicated by the black arrow in the lower right of Figure 6.

This noise rate was determined by summing the rates on the detector plane from the closest (to the central facet) 1/4 of the area of each of the four corner facets (those that share a corner with the central facet and are shielded behind aluminum blanks — see the small squares in the top panel of Figure 5). These are plotted as the light curves using black lines in Figure 6. Because of the cruciform arms from single reflections and the low-intensity diffuse region, the point spread function from X-rays that nominally hit the detector plane behind active facets can extend into areas on the detector plane that are behind blanked facets.[39] These are real X-rays that can, in principle, create a response behind blanked-off facets so that this rate is truly an upper limit on the noise level.

As can be seen in Figure 6, the observed DXL/STORM count rate over the entire rocket flight was about 1.5 Hz. This

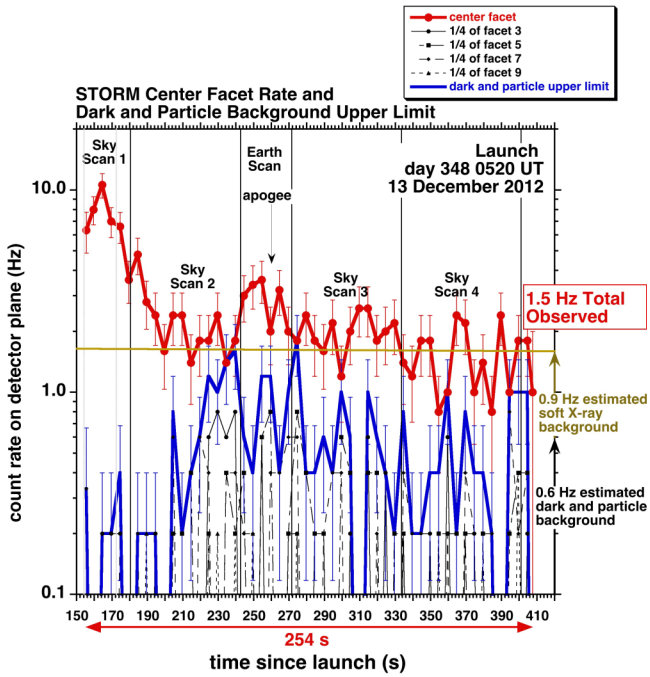

FIG. 6. The observed DXL/STORM light curve during the DXL flight. Sky scan 1 crossed a soft X-ray source at about 160 s.

rate is consistent with a 0.9 Hz rate due to soft X-rays and a 0.6 Hz background rate, as illustrated by the black and brown arrows at the lower right of Figure 6.

During rocket flights, the background rate typically increases with increasing altitude. Note that for DXL/STORM, the maximum dark and particle rate occurs near apogee around 250-270 s into the flight. Because DXL/STORM had no vetoing detectors to eliminate events due to penetrating particles, the variation in background we observe is consistent with the variation in particle flux during the flight with a maximum near apogee.

VI. SPATIAL IMAGING

Although the populated side facet discussed above was only partially sensitive, the data collected from this facet have been compared to those from the central populated facet. The data from these two facets are qualitatively similar, although the side facet count rate is a factor of five or so lower.

During sky scan one, a source of soft X-rays was observed by both the central and side facets. The peak rate of this source occurs later in the side facet than in the central facet. Furthermore, the centroid of the soft X-ray photons over this period shows systematic motion towards the side facet. During this period, the DXL FOV was moving from north toward the south ecliptic to scan through the helium focusing cone. The side facet was located on the north side of the central facet, so that this behavior is consistent with a spatially coherent stationary source moving through the DXL/STORM FOV from the central facet to the side facet as the rocket rotated toward the south ecliptic. The magnitude and rate of the observed source's angular motion is also consistent with this interpretation.

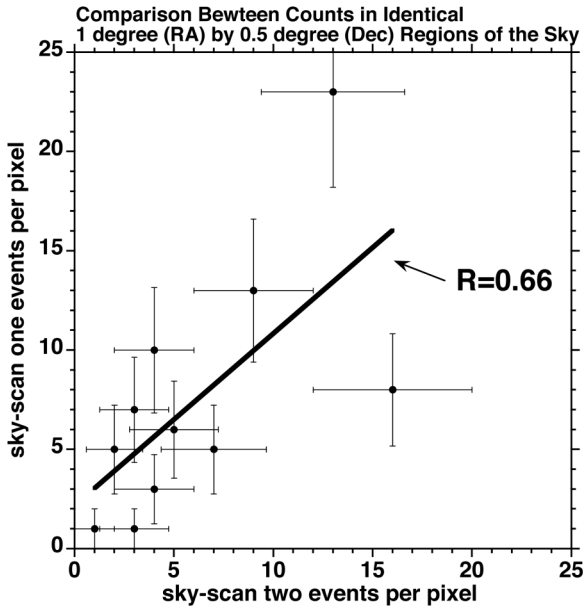

FIG. 7. The correlation between sky scan one and sky scan two events observed coming from the same regions of the sky. The eleven regions of the sky used are 1° in right ascension and 0.5° in declination.

Using orbit and attitude calculations supplied by Wallops Flight Facility, each photon observed by DXL/STORM over the course of the rocket flight was converted from instrument coordinates into sky coordinates (right ascension and declination) so that the count rates from similar regions of the sky can be compared directly. Some of the difficulties inherent in this comparison include the following: (i) the orbit and attitude calculations have an estimated absolute accuracy of about ±1° in each axis, although the repeatability of the measurements has an expected accuracy of less than 0.2° over the course of the entire flight (due to gyro drift), (ii) the scanning of the DXL rocket results in low statistics from any given region of the sky, (iii) there could have been some motion of the DXL/STORM instrument relative to its rocket section due to causes like non-perfectly rigid mounts and thermal shifts as the payload heats up and cools over time in flight, (iv) a non-uniform rotation rate could cause integration times to vary between scans and within scans, and (v) the putative DXL/STORM look direction may be off due to uncertainties in the mechanical mounting of the instrument, that is, misalignment of DXL/STORM both internally and externally.

In spite of these challenges, Figure 7 shows the events per pixel from similar regions of the sky in right ascension and declination for sky scan one (y-axis) and sky scan two (x-axis). The data are from the region of the sky having good observational overlap during the two sky scans, constituting eleven pixels, each of which is 1 degree in right ascension and 0.5° in declination. The correlation between the counts is 0.66 with a slope of 0.87, not unreasonable given the statistical uncertainty inherent in the number of counts in each pixel. Thus, in spite of the concerns listed above, the observations are consistent with DXL/STORM observing the same overall structure on the ~1° pixel level during sky scan two as it did during sky scan one.

The data shown in Figure 7 are from the region of the sky from about 159° to 165° right ascension and about 19° to 24° declination. The region was away from the scan endpoints and the rocket rotation was relatively constant during this period (~0.77°/s), so each pixel has roughly the same integration time. An examination of the ROSAT R12 band (0.111-0.284 keV) sky map in this region shows a non-uniformity of ~50% in the soft X-ray surface brightness exclusive of point sources. (We have examined the point sources in this region of the sky from the RASS catalog,[40] and none of these point sources appears to be strong enough to be observable by DXL/STORM.) However, there are other effects such as SWCX contributing to the scatter seen in Figure 7, so how much of the correlation external to the detector seen in Figure 7 can be attributed to the soft X-ray background is uncertain.

VII. CONCLUSION

Preliminary results from the DXL/STORM flight discussed here indicate the following: (1) the magnitude of the observed count rate is consistent with our pre-flight expectations based on the instrument look direction and the intensity of the soft X-ray background in this direction. Because DXL/STORM was viewing through the flank of the magnetosheath, the observed signal was not, and was not expected to be, dominated by magnetosheath SWCX, although it is almost certain some of the observed signal is from this source. For example, Figure 5 in Collier *et al.*[18] suggests that viewing perpendicular to the sun-earth line, as DXL/STORM was, the exospheric SWCX contribution can be a non-negligible fraction of the soft X-ray background. (2) From a comparison between the two populated facets as well as a statistical analysis correlating the counts observed in the same region of the sky between sky scan one and sky scan two, DXL/STORM did image structure in the observed soft X-rays.

Based on these results, it is clear that a wide FOV soft X-ray imager using the DXL/STORM design would successfully observe the intense magnetosheath and cusp SWCX soft X-ray emission present on the earth's dayside. For example, Robertson *et al.*,[7] Figure 4, right panel, suggests that for average solar wind conditions, the SWCX soft X-ray emission from the nose is at least twice that from the flank while the cusp emission is about twice the emission from the nose.

The development of a flight-proven prototype wide FOV soft X-ray camera represents an important milestone in establishing a global magnetosheath, cusp, and solar wind-planetary interaction imaging capability. The DXL/STORM instrument demonstrates proof-of-concept for a full-scale mission to study SWCX. Meanwhile, we look forward to a soft X-ray camera playing a central role on a future spacecraft, such as ESA's AXIOM.[30] Recently, the European Space Agency and the Chinese Academy of Sciences recommended the Solar wind Magnetosphere Ionosphere Link Explorer (SMILE) as their candidate for a collaborative science mission with an anticipated launch in 2021. SMILE includes a wide field-of-view soft X-ray imager using lobster-eye optics to globally image the terrestrial magnetosheath.

ACKNOWLEDGMENTS

Thanks to the Wallops Flight Facility and White Sands Missile Range personnel who supported the DXL mission, including DXL/STORM vibration testing, and were so generally helpful for DXL/STORM. Special thanks to Paul Rozmarynowski for mechanical design support, Kenneth Simms for assembly support, and Norman Dobson for GSE support. Also thanks to Steve Brown in the GSFC radiation facility for support for the proton beam testing and to Dan McCammon for pointing out useful references. The flight instrument development described in this paper was funded through the Planetary, Heliophysics, and Astrophysics Divisions at GSFC through Goddard's Internal Research and Development (IRAD) program. D.K. acknowledges financial support for her activity through the program "Soleil Héliosphère Magnétosphère" of the French space agency CNES and the National Program "Physique Chimie du Milieu Interstellaire" of the Institut National des Sciences de l'Univers (INSU).

[1]K. Kuntz, Y. Collado-Vega, M. Collier, H. Connor, T. Cravens, D. Koutroumpa, F. Porter, I. Robertson, D. Sibeck, S. Snowden, N. Thomas, and B. Walsh, "The solar wind charge-exchange production factor for hydrogen," Astrophys. J. (in press).
[2]T. E. Cravens, Geophys. Res. Lett. **24**, 105, doi:10.1029/96GL03780 (1997).
[3]D. G. Sibeck, G. Paschmann, R. A. Treumann, S. A. Fuselier, W. Lennartsson, M. Lockwood, R. Lundin, K. W. Ogilvie, T. G. Onsager, T.-D. Phan, M. Roth, M. Scholer, N. Sckopke, K. Stasiewicz, and M. Yamauchi, Space Sci. Rev. **88**, 207 (1999).
[4]M. R. Collier, D. G. Sibeck, T. E. Cravens, I. P. Robertson, and N. Omidi, EOS Trans. **91**, 213 (2010).
[5]J. A. Carter, S. Sembay, and A. M. Read, Mon. Not. R. Astron. Soc. **402**, 867 (2010); e-print arXiv:0911.0897 [astro-ph.HE].
[6]J. A. Carter, S. Sembay, and A. M. Read, Astron. Astrophys. **527**, A115 (2011); e-print arXiv:1101.1848 [astro-ph.IM].
[7]I. P. Robertson, M. R. Collier, T. E. Cravens, and M.-C. Fok, J. Geophys. Res.: Space Phys. **111**, A12105, doi:10.1029/2006JA011672 (2006).
[8]R. Wegmann and K. Dennerl, Astron. Astrophys. **430**, L33 (2005).
[9]C. Lisse, K. Dennerl, J. Englhauser, M. Harden, F. Marshall, M. Mumma, R. Petre, J. Pye, M. Ricketts, J. Schmitt, J. Trümper, and R. West, Science **274**, 205 (1996).
[10]R. Wegmann, K. Dennerl, and C. Lisse, Astron. Astrophys. **428**, 647 (2004).
[11]M. Holmström, S. Barabash, and E. Kallio, Geophys. Res. Lett. **28**, 1287, doi:10.1029/2000GL012381 (2001).
[12]K. Dennerl, Astron. Astrophys. **394**, 1119 (2002); e-print arXiv:astro-ph/0211215.
[13]H. Gunell, M. Holmström, E. Kallio, P. Janhunen, and K. Dennerl, Geophys. Res. Lett. **31**, L22801, doi:10.1029/2004GL020953 (2004).
[14]H. Gunell, M. Holmström, E. Kallio, P. Janhunen, and K. Dennerl, Adv. Space Res. **36**, 2057 (2005).
[15]K. Dennerl, C. M. Lisse, A. Bhardwaj, V. Burwitz, J. Englhauser, H. Gunell, M. Holmström, F. Jansen, V. Kharchenko, and P. M. Rodríguez-Pascual, Astron. Astrophys. **451**, 709 (2006).
[16]K. Dennerl, V. Burwitz, J. Englhauser, C. Lisse, and S. Wolk, Astron. Astrophys. **386**, 319 (2002); e-print arXiv:astro-ph/0204237.
[17]K. Dennerl, Planet. Space Sci. **56**, 1414 (2008).
[18]M. R. Collier, S. L. Snowden, M. Sarantos, M. Benna, J. A. Carter, T. E. Cravens, W. Farrel, S. Fatemi, H. K. Hills, R. Hodges, M. Holmström, K. D. Kuntz, F. S. Porter, A. Read, I. Robertson, S. Sembay, D. Sibeck, T. Stubbs, P. Travnicek, and B. Walsh, J. Geophys. Res.: Planets **119**, 1, doi:10.1002/2014JE004628 (2014).
[19]D. Koutroumpa, M. Collier, K. Kuntz, R. Lallement, and S. Snowden, Astrophys. J. **697**, 1214 (2009).
[20]I. P. Robertson and T. E. Cravens, J. Geophys. Res.: Space Phys. **108**, 8031, doi:10.1029/2003JA009873 (2003).
[21]K. D. Kuntz, AIP Conf. Proc. **1156**, 3 (2009).
[22]A. N. Brunton, G. W. Fraser, J. E. Lees, and I. C. E. Turcu, Appl. Opt. **36**, 5461 (1997).
[23]G. W. Fraser, A. N. Brunton, N. P. Bannister, J. F. Pearson, M. Ward, T. J. Stevenson, D. J. Watson, B. Warwick, S. Whitehead, P. O'Brian, N. White, K. Jahoda, K. Black, S. D. Hunter, P. Deines-Jones, W. C. Priedhorsky, S. P. Brumby, K. N. Borozdin, T. Vestrand, A. C. Fabian, K. A. Nugent, A. G. Peele, T. H. Irving, S. Price, S. Eckersley, I. Renouf, M. Smith, A. N. Parmar, I. M. McHardy, P. Uttley, and A. Lawrence, Proc. SPIE **4497**, 115–126 (2002).
[24]M. Galeazzi, M. Chiao, M. R. Collier, T. Cravens, D. Koutroumpa, K. D. Kuntz, R. Lallement, S. T. Lepri, D. McCammon, K. Morgan, F. S. Porter, I. Robertson, S. L. Snowden, N. E. Thomas, Y. Uprety, E. Ursino, and B. M. Walsh, Nature **512**, 171 (2014).
[25]P. Kirkpatrick and A. V. Baez, J. Opt. Soc. Am. **38**, 766 (1948).
[26]G. Price, A. Brunton, M. Beijersbergen, G. Fraser, M. Bavdaz, J.-P. Boutot, R. Fairbend, S.-O. Flyckt, A. Peacock, and E. Tomaselli, Nucl. Instrum. Methods Phys. Res., Sect. A **490**, 276 (2002).
[27]M. R. Collier, F. S. Porter, D. G. Sibeck, J. A. Carter, M. P. Chiao, D. J. Chornay, T. Cravens, M. Galeazzi, J. W. Keller, D. Koutroumpa, K. Kuntz, A. M. Read, I. P. Robertson, S. Sembay, S. Snowden, and N. Thomas, Astron. Nachr. **333**, 378 (2012).
[28]G. W. Fraser, J. D. Carpenter, D. A. Rothery, J. F. Pearson, A. Martindale, J. Huovelin, J. Treis, M. Anand, M. Anttila, M. Ashcroft, J. Benkoff, P. Bland, A. Bowyer, A. Bradley, J. Bridges, C. Brown, C. Bulloch, E. J. Bunce, U. Christensen, M. Evans, R. Fairbend, M. Feasey, F. Giannini, S. Hermann, M. Hesse, M. Hilchenbach, T. Jorden, K. Joy, M. Kaipiainen, I. Kitchingman, P. Lechner, G. Lutz, A. Malkki, K. Muinonen, J. Näränen, P. Portin, M. Prydderch, J. S. Juan, E. Sclater, E. Schyns, T. J. Stevenson, L. Strüder, M. Syrjasuo, D. Talboys, P. Thomas, C. Whitford, and S. Whitehead, Planet. Space Sci. **58**, 79 (2010).
[29]A. Martindale, J. F. Pearson, C. Whitford, G. W. Fraser, D. A. Rothery, D. Talboys, J. D. Carpenter, T. Stevenson, E. Bunce, R. Fairbend, J. Seguy, E. Sclater, I. Delgado, A. Dixon, J. Treis, J. M. Mas-Hesse, J. L. San Juan, K. Muinonen, C. Sawyers, C. Bulloch, and E. Schyns, Proc. SPIE **7441**, 744115 (2009).
[30]G. Branduardi-Raymont, S. Sembay, J. Eastwood, D. Sibeck, T. Abbey, P. Brown, J. Carter, C. Carr, C. Forsyth, D. Kataria, S. Kemble, S. Milan, C. Owen, L. Peacocke, A. Read, A. Coates, M. Collier, S. Cowley, A. Fazakerley, G. Fraser, G. Jones, R. Lallement, M. Lester, F. Porter, and T. Yeoman, Exp. Astron. **33**, 403 (2012).
[31]F. Jansen, D. Lumb, B. Altieri, J. Clavel, M. Ehle, C. Gabriel, M. Guainazzi, P. Gondoin, R. Much, R. Munoz, M. Santos, N. Schartel, D. Texier, and G. Vacanti, Astron. Astrophys. **365**, L1 (2001).
[32]C. Martin, P. Jelinsky, M. Lampton, R. Malina, and H. Anger, Rev. Sci. Instrum. **52**, 1067 (1981).
[33]M. Galeazzi, M. Chiao, M. R. Collier, T. Cravens, D. Koutroumpa, K. D. Kuntz, S. Lepri, D. McCammon, F. S. Porter, K. Prasai, I. Robertson, S. Snowden, and Y. Uprety, Exp. Astron. **32**, 83 (2011); e-print arXiv:1108.0418 [astro-ph.SR].
[34]M. Galeazzi, M. R. Collier, T. Cravens, D. Koutroumpa, K. D. Kuntz, S. Lepri, D. McCammon, F. S. Porter, K. Prasai, I. Robertson, S. Snowden, N. E. Thomas, and Y. Uprety, Astron. Nachr. **333**, 383 (2012).
[35]J. A. Carter and S. Sembay, Astron. Astrophys. **489**, 837 (2008); e-print arXiv:0807.3624.
[36]T. E. Cravens, I. P. Robertson, and S. L. Snowden, J. Geophys. Res. **106**, 24883, doi:10.1029/2000JA000461 (2001).
[37]K. Kuntz and S. Snowden, Astrophys. J. **543**, 195 (2000).
[38]S. Pearce, J. Lees, J. Pearson, G. Fraser, A. Brunton, K. Flanagan, A. Kenter, M. Barbera, V. Dhanak, A. Robinson, and D. Teehan, Proc. SPIE **2518**, 322 (2010).
[39]J. K. Black, A. N. Brunton, N. P. Bannister, P. Deines-Jones, and K. Jahoda, Nucl. Instrum. Methods Phys. Res., Sect. A **513**, 123 (2003).
[40]W. Voges, B. Aschenbach, T. Boller, H. Bräuninger, U. Briel, W. Burkert, K. Dennerl, J. Englhauser, R. Gruber, F. Haberl, G. Hartner, G. Hasinger, M. Kürster, E. Pfeffermann, W. Pietsch, P. Predehl, C. Rosso, J. H. M. M. Schmitt, J. Trümper, and H. U. Zimmerman, Astron. Astrophys. **349**, 389 (1999).